Electronic Supplementary Material (ESI) for CrystEngComm.
This journal is © The Royal Society of Chemistry 2015

ESI

Star-shaped VO_2 (M) Nanoparticles Film with High Thermochromic Performance†

Li Zhong, Ming Li, Hua Wang, Yuanyuan Luo, Jing Pan and Guanghai Li*

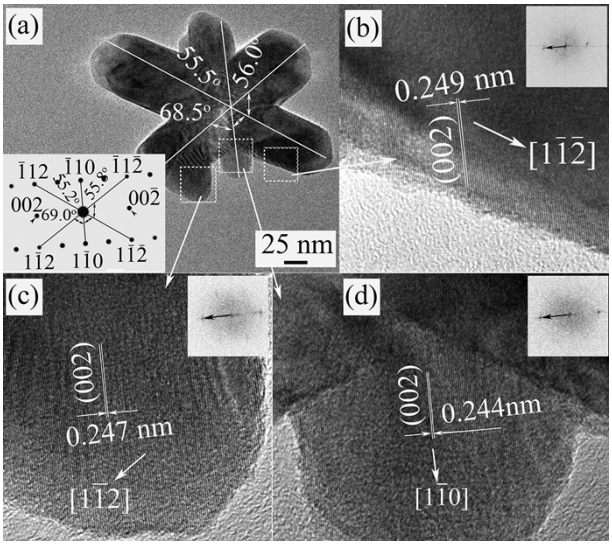

Fig. S1. (a) TEM image of a star-shaped VO_2 (D) NP, (b-c) HRTEM image and the corresponding FFT pattern (the inset) of the areas indicated in (a). The growth directions and orientation angles are shown in (a), the down left inset in (a) is the corresponding simulation SAED pattern of VO_2 (D) single crystal from [110] zone axis.

One can see that the star-shaped VO_2 (D) NP is composed of three intersected nanorods with different orientation angles. The lattice fringes of about 0.24 nm in the lower three arms in Fig. 2a agree well with the spacing of the (002) lattice plane of monoclinic VO_2 (D), and the corresponding fast Fourier transform (FFT) patterns in the insets also proved that these lattice fringes belong to (002) lattice planes. From the crystallographic symmetry and orientation angels of monoclinic VO_2 (D) we deduce that the growth direction of these three arms might be along $[1\bar{1}0]$, $[1\bar{1}2]$ and $[1\bar{1}\bar{2}]$, as shown in Fig. 2a. The measured angles between the growth direction of the adjacent arms match well with the theoretical values (the inset in Fig. 2a, from $[110]$ zone axis). From this result we speculated that the intersected interfaces of the star-shaped VO_2 (D) NPs are {112} planes, and the arms grow along $\langle 110 \rangle$ and $\langle 112 \rangle$ directions. Further experiments are needed to confirm the crystallographic correlation among the six arms in the star-shaped VO_2 (D) NPs.

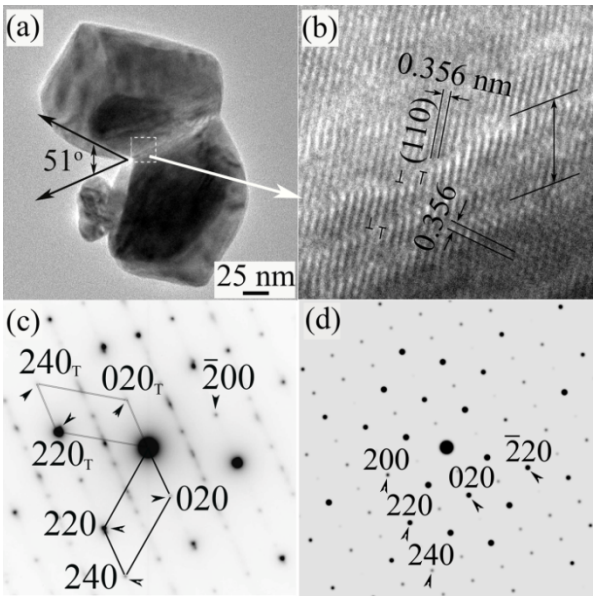

Fig. S2 (a) TEM image, (b) HRTEM image, (c) the corresponding SAED pattern of two intersecting arms in a broken star-shaped VO_2 (D) NP. (d) Simulation SAED pattern of VO_2 (D) single crystal from [001] zone axes. The double arrow zone in the (b) is the transition zone of the two arms consisting of some dislocations.

The lattice fringes of about 0.356 nm, which are perpendicular to growth direction of the NPs shown in Fig. S2b, can be assigned to the (110) atomic plane. The corresponding SAED pattern shown in Fig. S2c proved that the NPs grow along [110] direction and the twin plane is (020) atomic plane, which is in a good agreement with the simulation SAED pattern of VO_2 (D) single crystal from [001] zone axis shown in Fig. S2d. The (020) twin can be crystallographically described by about 51° rotation to the twin plane. The twining on (020) plane is possible as there are some dislocations in the transition area due to local inhomogeneous deformation, see the marked lines in Fig. S2b.

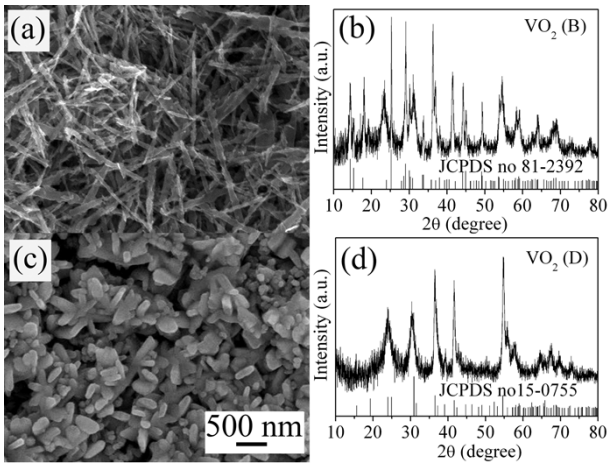

Fig. S3. FESEM image and the corresponding XRD pattern of the products hydrothermal synthesis for two days at temperature of (a, b) 180 °C (VO_2 (B) nanobelts), and (c, d) 220 °C (star-shaped VO_2 (D) NPs).

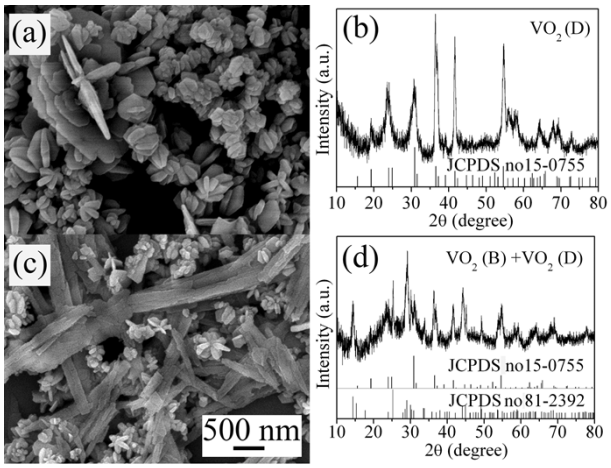

Fig. S4. FESEM images and the corresponding XRD pattern of product hydrothermal synthesis at 200 ºC for two days with surfactant of (a, b) PVP (star-shaped VO_2 (D) NPs) and (c, d) CTAB (VO_2 (D) NPs and VO_2 (B) nanobelts.)

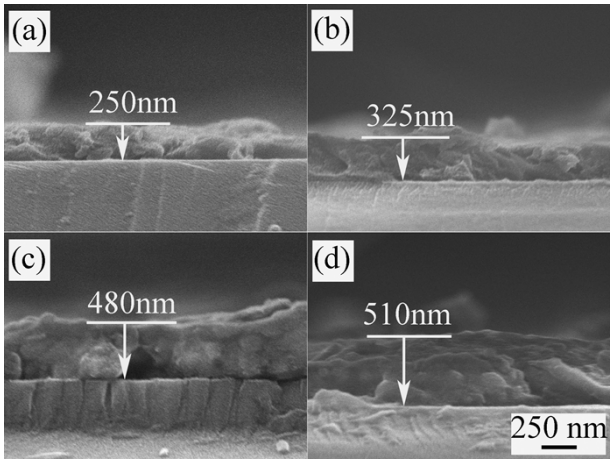

Fig. S5. Cross section FESEM images of VO_2 (M) nanoparticles thin films on glass substrate with the thickness of (a) 250, (b) 325, (c) 480 and (d) 510 nm.

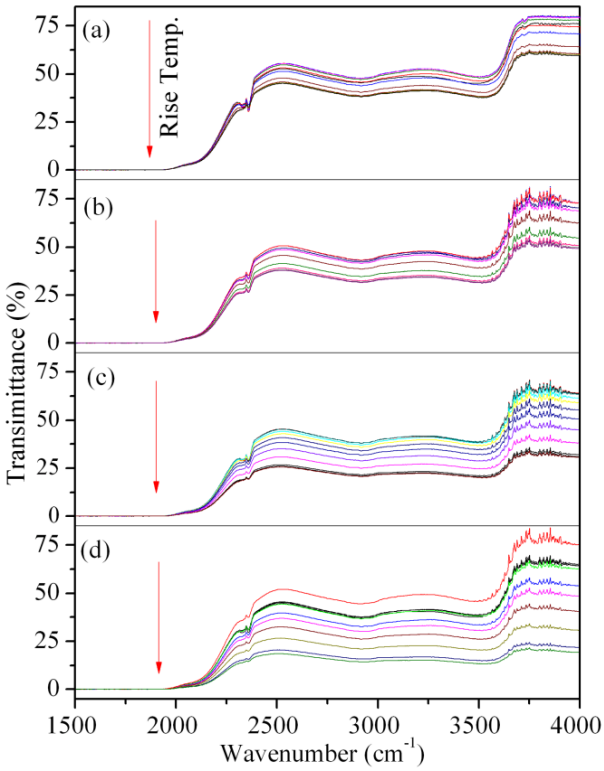

Fig. S6. Variable-temperature FT-IR spectra of the VO_2 (M) nanoparticles thin film on glass substrates before and after phase transition with the thickness of (a) 250, (b) 325, (c) 480 and (d) 510 nm.

Noting that the optical opaque phenomena at wavenumbers below 2000 cm^{-1} (5 μm) is caused by the intensive absorption of glass substrate.

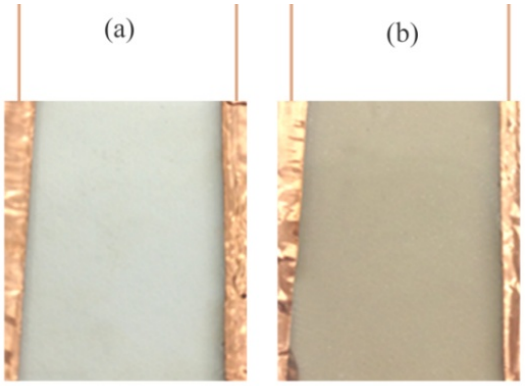

Fig. S7. Optical photos of (a) Ag NWs transparent conducting film heater and (b) VO_2 NPs/Ag NWs/glass device.

The Ag NWs film heater has nearly the same transparent as glass substrate (Fig. S7a), and after spin-coating with VO_2 (M) NPs on top of the film heater, the colour of the device become brown (Fig. S7b).

Table 1 Integrated luminous and solar irradiation transmittance of VO_2 (M) NPs films

Thickness (nm)	T_{lum} (%, 25 °C)	T_{lum} (%, 100 °C)	T_{sol} (%, 25 °C)	T_{sol} (%, 100 °C)	ΔT_{sol} (%)
250	51.75	57.23	62.90	61.82	1.08
325	42.97	44.18	54.91	47.49	7.32
480	22.49	28.9	36.17	30.89	5.28
510	7.37	11.52	21.57	14.19	7.36

When used as smart window coating for the VO_2 (M) NPs thin films, a considerable integrated luminous transmittance and a proper modulation ability of solar transmittance is required. The integrated luminous (lum) and solar (sol) irradiation transmittance are obtained from the following formula:

$$T_i(\lambda) = \int \varphi_i(\lambda) T(\lambda,\tau) d\lambda / \int \varphi_i(\lambda) d\lambda \qquad (1)$$

where T is transmittance, λ is the wavelength of the incident light, i denotes lum or sol, φ_{lum} is the spectral sensitivity of the light-adapted human eye, and φ_{sol} is the solar irradiance spectrum for air mass 1.5, see detail in reference [1]. The calculated results are shown in Table S1, from which one can see that the T_{lum} (360–830 nm) and T_{sol} (350–2400 nm) decreases with increasing the film thicknesses at both 25 °C and 100 °C, while the modulation ability of solar transmittance (ΔT_{sol} =T_{sol} (25 °C) - T_{sol} (100 °C)) increases except the film with the thickness of 325 nm. One also can see that the 325 nm film shows a relative uniform luminous transmittance at both low and high temperatures.

[1] J. Du, Y. F.Gao, Z. Chen, L. T. Kang, Z. T.Zhang, H. J. Luo, Solar Energy Mater. & Solar Cells 2013, 110, 1–7.